ELSEVIER

Earth and Planetary Science Letters 205 (2002) 25–35

EPSL

www.elsevier.com/locate/epsl

The 660-km discontinuity within the subducting NW-Pacific lithospheric slab

Sergei Lebedev [a,*], Sébastien Chevrot [a,b], Rob D. van der Hilst [a]

[a] *MIT, EAPS, 54-512, Cambridge, MA 02139, USA*
[b] *Observatoire Midi Pyrénées, 14 Avenue Edouard Belin, 31400 Toulouse, France*

Received 23 May 2002; received in revised form 11 September 2002; accepted 9 October 2002

Abstract

The 660-km seismic discontinuity (*660*) in Earth's mantle is generally attributed to the breakdown of the ringwoodite phase of olivine, but other mineral reactions are also thought to occur near 660-km depth. Recently, complex arrivals of *P*660*s* waves (converted from *P* to *s* at the *660*) in active and recently active subduction zones have been interpreted as evidence for additional seismic discontinuities caused by the garnet–perovskite and garnet–ilmenite–perovskite phase transformations ($gt \rightarrow pv$, $gt \rightarrow il \rightarrow pv$) at relatively low temperatures. Here we show that the *P*660*s* phases converting at the *660* within the subducting NW-Pacific slab beneath the station MDJ in Northeast China are clear and coherent, with no additional arrivals in the vicinity. *P*660*s* waves that convert near the boundaries of the area where the *660* occurs within the slab produce distinctly more complex, multiple arrivals, but they are more likely to be caused by small-scale topography rather than 'multiplicity' of the *660*. Our observations suggest that the $gt \rightarrow pv$ transformation and the $gt \rightarrow il \rightarrow pv$, if it occurs in the mantle, are spread over tens of kilometers and do not have sharp onsets visible to short-period seismic waves.
© 2002 Elsevier Science B.V. All rights reserved.

Keywords: transition zone; phase transformations; converted waves; heterogeneity; topography

1. Introduction

The seismic discontinuity at a global average depth of 660 km in the Earth's mantle (the *660*) has been attributed to the transformation of ringwoodite (γ-phase of olivine) into perovskite and magnesiowüstite ($\gamma \rightarrow pv+mw$) [1–5]. Other mineral reactions may also occur close to 660-km depth, some of them only at certain ambient temperature and composition [6]. Near 750-km depth, garnet (*gt*) is thought to transform into perovskite (*pv*) [7]. At anomalously low temperatures (such as in subduction zones) garnet may transform into ilmenite (*il*) and ilmenite into perovskite in the 600–750-km depth range [8]. The transformations could give rise to two additional seismic discontinuities in the vicinity of the *660*. An observation of seismic waves converted at interfaces near the *660* would be indicative of the occurrence of $gt \rightarrow il \rightarrow pv$ and could provide constraints on the effective sharpness [7] of the transformations. An

* Corresponding author. Fax: +1-617-258-9697.
E-mail address: sergei@quake.mit.edu (S. Lebedev).

0012-821X/02/$ – see front matter © 2002 Elsevier Science B.V. All rights reserved.
PII: S0012-821X(02)01011-7

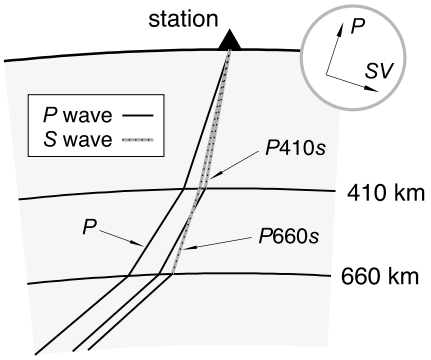

Fig. 1. Schematic ray diagram of the *P*, *P*410*s*, and *P*660*s* waves in a laterally homogeneous mantle. Triangle denotes the seismic station on the Earth's surface. The axes *P* and *SV* (top right) are in the direction of the P and SV waves' particle motion.

absence of pertinent seismic phases would suggest that the transformations – if at all present – are spread over large depth intervals and do not have sharp onsets.

Pds arrivals are produced by deep-turning compressional waves *P* converted to upgoing shear waves *s* at a depth *d* (Fig. 1) and are extensively used in studies of upper mantle discontinuities [9–12]. In active or recently active subduction zones, however, *P*660*s* waveforms can be difficult to interpret because of their complexity, caused by the effects of small-scale topography on the *660* and strong seismic-velocity heterogeneity in the upper mantle above it (e.g. [12,13]). Assuming that the lateral heterogeneity is absent or insignificant, one could then erroneously attribute the *P*660*s*-waveform complexity to structure of the *660* itself. Recently, multiple peaks near *P*660*s* arrivals on seismic records have been interpreted as *Pds* waves converted from multiple interfaces near 660-km depth, which in turn was interpreted as evidence for the occurrence of sharp $gt \rightarrow il$, $il \rightarrow pv$, and $gt \rightarrow pv$ [14–16].

Here we analyze *P*660*s* waves recorded at the station MDJ, Mudanjiang, of the Chinese Digital Seismic Network, a top-quality station situated above the region where the shallow-angle NW-Pacific slab reaches the *660*. We observe that the waves converting at the *660* well within the slab form clear single arrivals. In contrast, *P*660*s* converting where the boundaries of the slab cross the discontinuity exhibit complex waveform patterns that vary consistently with location of the conversion points relative to the slab. These observations strongly suggest that the waveform complexity is a result of wave-propagation effects rather than conversion at multiple discontinuities. The absence of multiple arrivals from within the slab indicates that the $gt \rightarrow il \rightarrow pv$ transformations – if present – are wide and smooth.

2. Data

Station MDJ (Fig. 2) has produced high-quality recordings since 1986. Below the station, the subducting NW-Pacific lithospheric slab reaches the *660* and, according to high-resolution tomography [17–19], penetrates into the lower mantle (Fig. 3). Because the subduction angle is shallow, the slab arrives at the *660* at a lateral distance of more than 1000 km away from the trench. Consequently, *P*660*s* waves on their way to the station travel little through the slab and not at all through the highly heterogeneous volcanic-arc

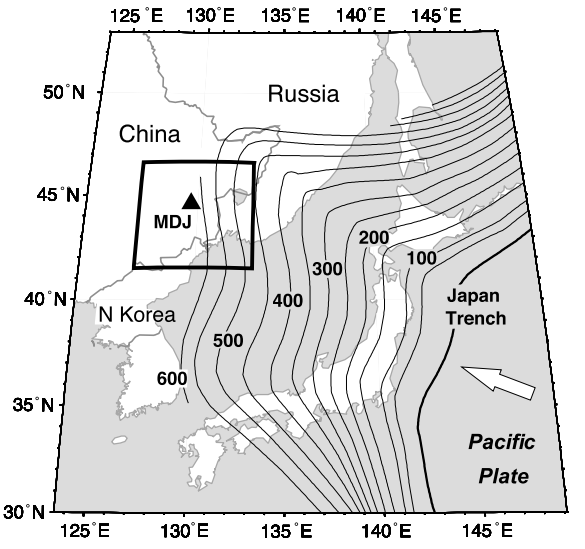

Fig. 2. The location of station MDJ (triangle) and the study region (bold lines). Arrow shows the motion of the Pacific plate relative to Eurasia. Contours of the depth (km) to the top of the seismogenic zone in the subducting slab are from [20] (based on hypocenters from [25]).

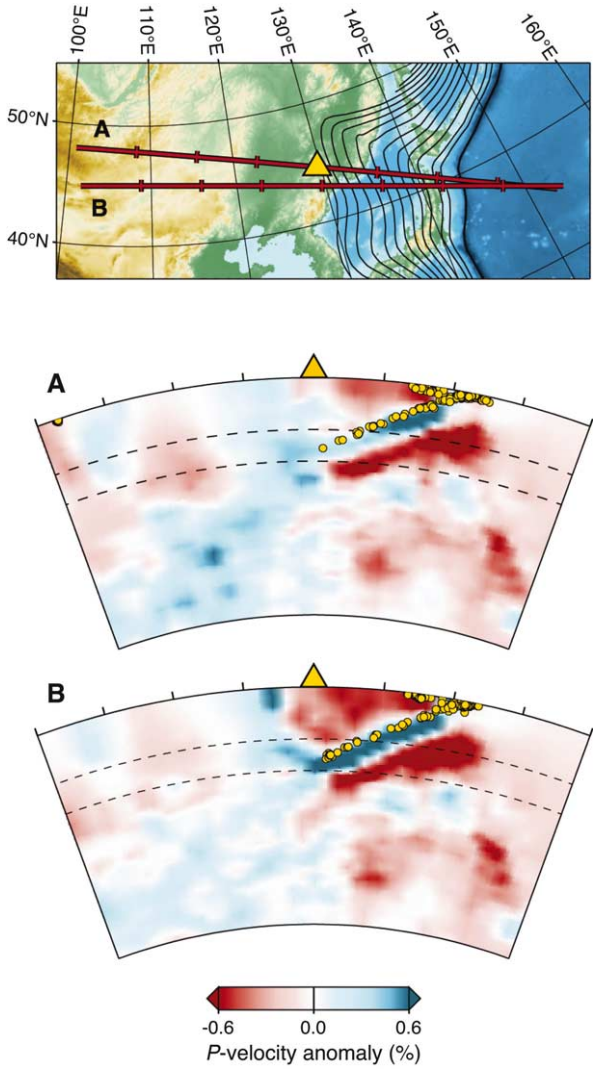

Fig. 3. Cross-sections through the tomographic model of [19] centered at our study region. Tick spacing is 5°. Earthquakes within 30 km of the cross-section planes are plotted as circles; hypocenters are from [25]. The reference model is *ak*135 [26].

shallow mantle. In comparison to island-arc stations, MDJ registers *P*660*s* phases that are weakly distorted by shallow structure and preserve information on the *660* itself. Other broadband stations above currently subducting, shallow-angle slabs within the transition zone have been temporary (short deployment time, lower signal to noise ratios) stations (e.g., in western South America), which makes MDJ uniquely suited for this study.

Following [9,12], we transform three-component broadband seismograms from MDJ into series of 'bumps' by means of rotation and deconvolution by the principal component of the recorded *P* wave train, with a move-out correction applied according to the slowness of the *P* wave. We discard traces with strong background noise before the *P* onset, with a prominent phase (*PcP*, *PP*) in the coda of the *P* wave, and with the SV-component (Fig. 1) amplitude exceeding 15% of that of the *P* wave after rotation and deconvolution. With a 2-s low-pass (fourth-order Butterworth) filter, 134 traces pass our selection criteria.

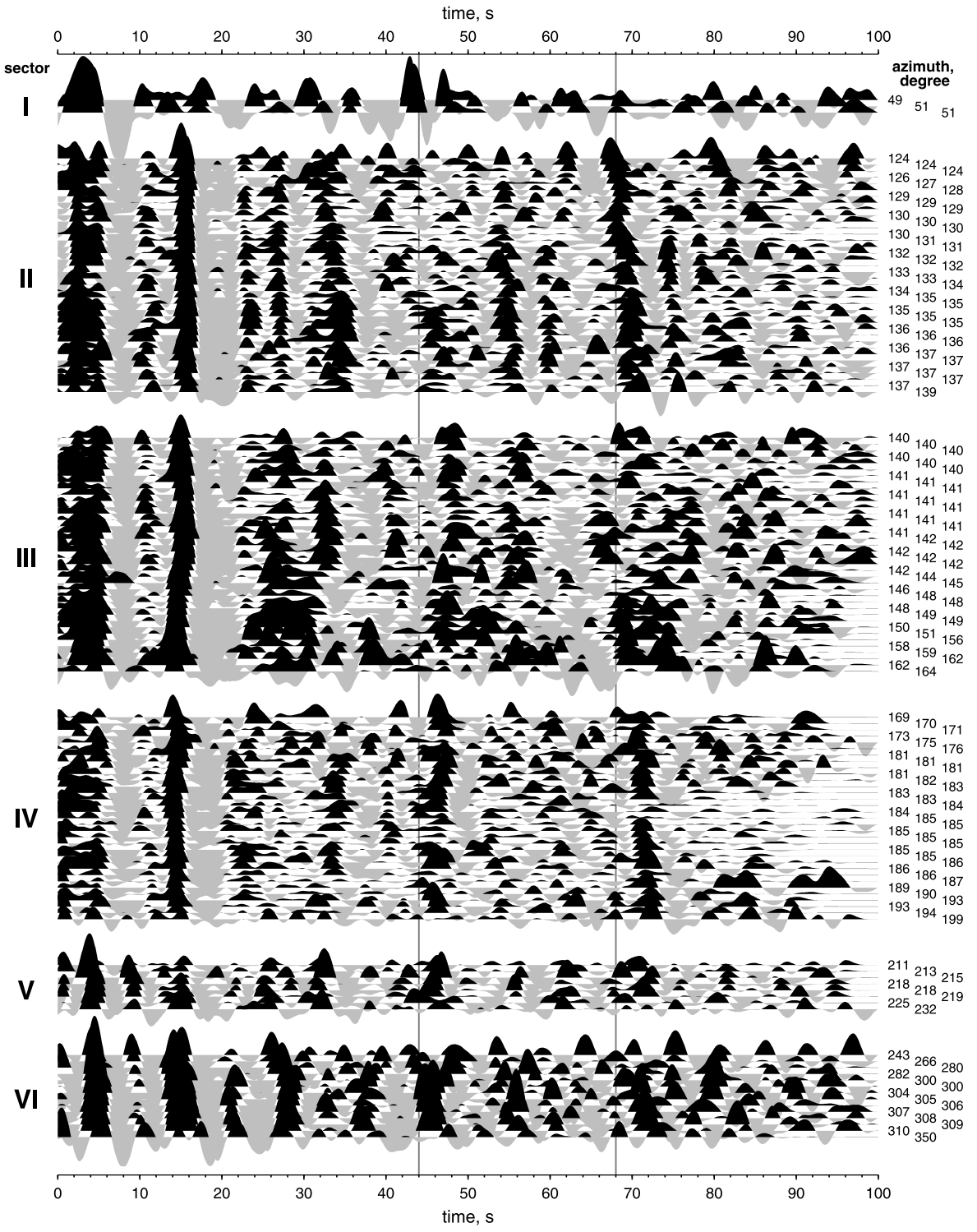
time, s
0
10
20
30
40
50
60
70
80
90
100
sector
azimuth, degree
I
II
III
IV
V
VI
49 51 51
124 124 124
126 127 128
129 129 129
130 130 130
130 131 131
132 132 132
133 133 134
134 135 135
135 135 135
136 136 136
136 137 137
137 137 137
137 139
140 140 140
140 140 140
141 141 141
141 141 141
141 141 141
141 142 142
142 142 142
142 144 145
146 148 148
148 149 149
150 151 156
158 159 162
162 164
169 170 171
173 175 176
181 181 181
181 182 183
183 183 184
184 185 185
185 185 185
185 185 186
186 186 187
189 190 193
193 194 199
211 213 215
218 218 219
225 232
243 266 280
282 300 300
304 305 306
307 308 309
310 350

These traces also pass the criteria with 4- and 6-s filters that we shall also use in the analysis.

Fig. 4 shows the records low-passed at 4 s and ordered by back azimuth (the angle between the directions from the station to the North and to the event). Comparing the *Pds* waveforms at neighboring azimuths we find that the records split in a few groups (sectors). In each of the six sectors in Fig. 4 the *P*660*s* arrivals are either coherent for most traces (Sectors II and IV) or scattered over a time interval with a distinct pattern of the scatter (upper and lower portions of Sector III exhibit different patterns of *P*660*s*-arrival scatter but for the purposes of our discussion can be grouped together).

In Fig. 5 we map the ray-theoretical conversion points of *Pds* at the *660* and the 410-km discontinuity (*410*). We also plot the estimated extent of the area where the slab penetrates through the *660*. For this estimate we extrapolated the contours of the top of the slab's seismogenic zone [20], assuming that they map the top of the slab itself (this assumption is supported by the slab image in Fig. 3). We defined the upper and lower boundaries of the slab as the surfaces with a 200 K temperature anomaly and, adopting the thermal slab model from [21], estimated that the slab thickness (distance between the two surfaces) in the lower transition zone is 100 km. With the Clapeyron slope of the $\gamma \rightarrow pv+mw$ transformation equal to −2.0 MPa/K [22], this implied a depression of the *660* by 10 km where thus defined slab's boundaries intersect it. These assumptions gave us the thin-striped area on Fig. 5. If the slab did not deform near the *660*, this area would approximate the region of the slab penetration into the lower mantle. Fig. 6 shows a schematic cross-section through the slab, with idealized rays of *P*660*s* waves coming from Sectors II–V superimposed.

The actual configuration of the slab may be more complex, with possible deformation near the *660*. The model of [19] suggests that the slab thickens laterally atop the discontinuity so that the western boundary of the region where the *660* occurs within the slab material is 100–200 km west of the station's longitude. Other tomographic models confirm the occurrence of such deformation (cross-sections through the MDJ region can be found in [17,18]). We account for this by expanding the slab-penetration region to include the thick-striped region, west of the thin-striped one. Regardless of the method used to map the slab, all or almost all conversion points in Sector IV are within the central and western – presumably, coldest – portions of the slab.

Clear, coherent *P*660*s* arrivals are observed in Sectors II and IV, near 69.0 and 71.4 s, respectively (Fig. 4). In Sector IV, the conversion points are within the central and western parts of the slab (Figs. 5 and 6). In Sector II, ray-theoretical conversion points at the *660* are just outside or at the boundary of the slab; the *P*660*s* arrivals in this sector are followed by two or three other coherent arrivals (Fig. 4). Sector III includes the eastern boundary of the slab, and the *P*660*s* waves converted in it form incoherent multiple peaks scattered over a wide interval between 66 and 78 s. In Sector V on the other side (to the west) of the slab, *P*660*s* waveforms are also distinctly different from and less coherent than those in Sector IV.

Examination of individual traces in Fig. 4 and the location of corresponding conversion points in Fig. 5 suggests that *P*660*s* waves that convert at the *660* near the boundaries of the slab have complex waveforms with multiple peaks, whereas the *P*660*s* with conversion points well within the slab form simple single peaks. The pattern remains the same on the stacks of the traces within each sector (Fig. 7) and is especially clear on shorter-period stacks (2- and 4-s low-pass filters). If the multiple peaks observed in Sectors III and V near the expected *P*660*s* arrival time were due to *P*-to-*s* conversions at different discontinuities (associated with both the $\gamma \rightarrow pv+mw$ and $gt \rightarrow il \rightarrow pv$ transformations), then they would be observed in Sec-

←

Fig. 4. Processed traces at station MDJ, ordered by azimuth and separated into six groups with similar *Pds*-arrival appearance in each. The traces are normalized by the *P*-wave amplitude. Time is measured from the *P*-wave arrival. Global-average arrival times of *P*410*s* and *P*660*s* are marked at 44 and 68 s.

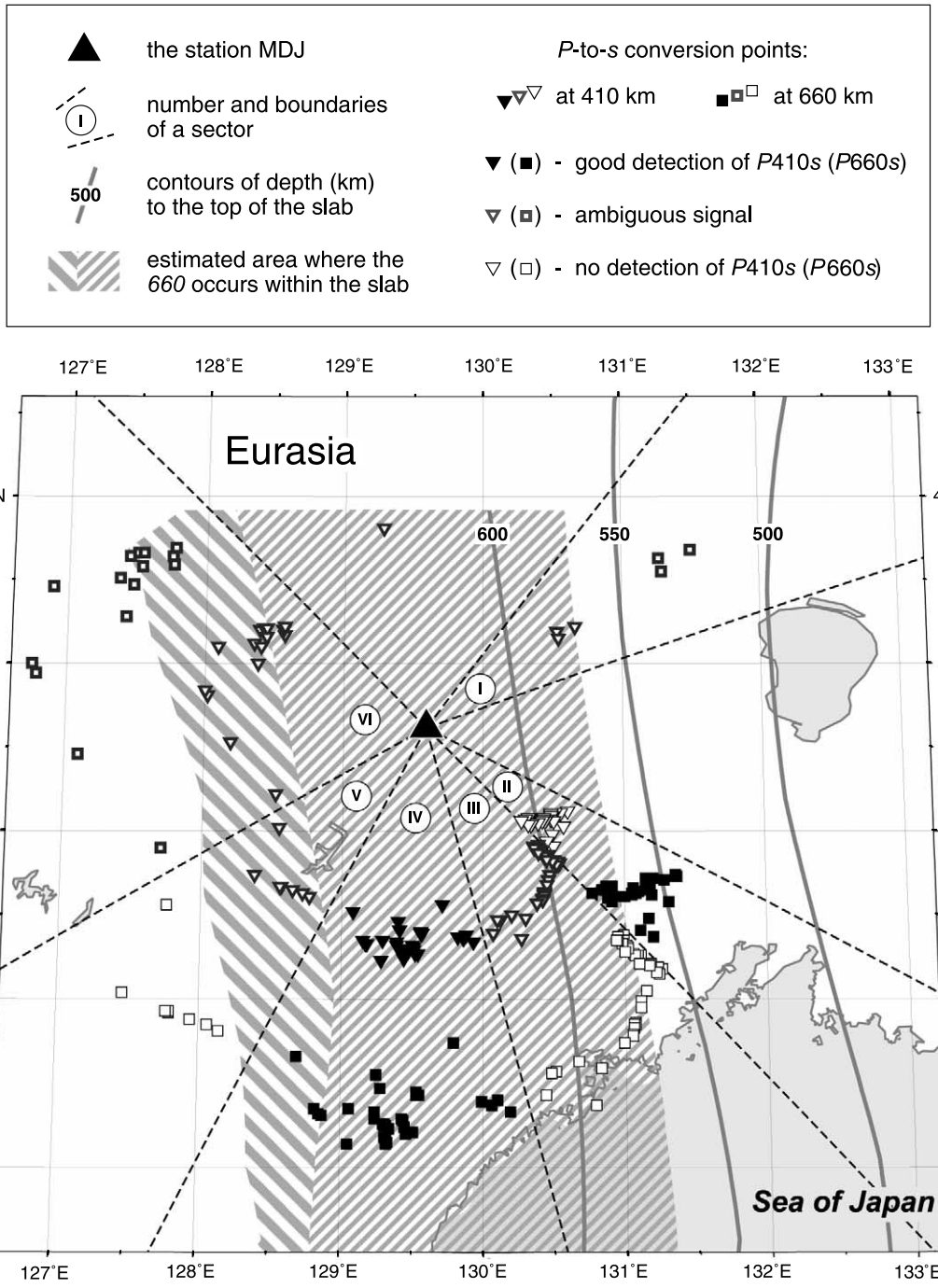

Fig. 5. The location of the station MDJ and ray-theoretical *P*-to-*s* conversion points at *410* (inverted triangles) and *660* (squares) computed in iasp91 [27]. The six sectors correspond to the six groups of traces in Fig. 4. Slab contours are from [20]. Within the striped area, the estimated depression of the *660* exceeds 10 km (see text). The location of the map area relative to the NW-Pacific trenches is shown in Fig. 2 (bold lines).

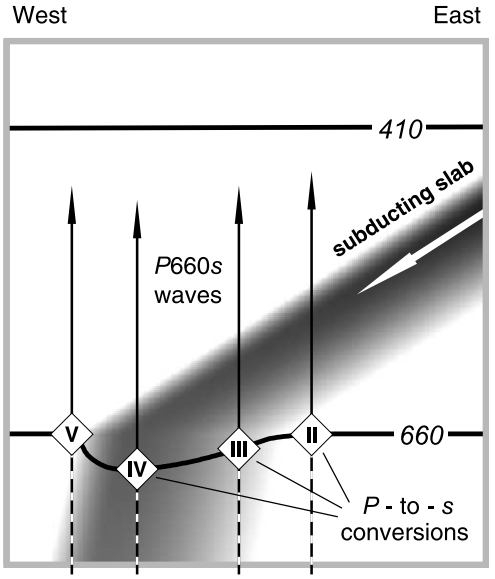

Fig. 6. Idealized rays of the *P*660*s* waves that sample the *660* within and near the subducting slab. *P* waves (dashed lines) convert to *s* waves (solid lines) at different points (diamonds) on the *660*. Roman numerals in the diamonds identify the sectors (as defined in Figs. 4 and 5) within which the conversions occur. Within the slab body, darker shade indicates lower temperature; the magnitude of the *660* depression is proportional to the thermal anomaly.

tor IV also, because the $gt \rightarrow il \rightarrow pv$ transformations are thought to occur at low temperatures and Sector IV covers the coldest part of the slab. This is not what we observe, and the data suggest a different explanation for the waveform complexity, namely, complexity of wave propagation caused by the topography on the *660*.

3. Discussion

Quantitative interpretation of *Pds* data have so far largely relied on the assumption of lateral homogeneity of the mantle beneath the station and, consequently, the assumption that a *P*-to-*s* conversion at a discontinuity (e.g., *660* or *410*) produces a single seismic arrival (*P*660*s* or *P*410*s*) (Fig. 1). If the actual seismic-velocity heterogeneity is weak and topography on discontinuities is small, the assumptions are still appropriate (generally more so for stacks of many traces than for individual records).

If small-scale topography on discontinuities is substantial, the assumptions are no longer valid, and a single interface may give rise to multiple peaks in both individual and stacked waveforms. Numerical experiments with realistic finite-frequency waves [13] have shown that a *660* topography with a 30-km peak-to-peak amplitude and a 100–400-km wavelength can produce splitting of the *P*660*s* peak into two, three, or more peaks, as well as a disappearance of the *P*660*s* arrival altogether. Because the amplitude of the *660* topography in the areas around subducted slabs is likely to reach 30 km (e.g., [3,23,24]), multiplicity of the *P*660*s* arrivals is an expected result of multipathing.

The ray-theoretical conversion points of *P*660*s* in our Sector IV are only 200–250 km away from those in Sector II (Fig. 5), but the *P*660*s* arrivals are 2–3 s later in IV compared to II (Fig. 4), which is consistent with the presence of strong *660* topography. On the stacks of all traces in Fig. 7 (2- and 4-s filters), the coherent arrivals from these two sectors are still visible and produce two distinct peaks. In this case, the reason for the apparent splitting of the *P*660*s* peak is obvious: azimuthal variation in the arrival time of a simple single peak.

The first report of the *660* 'multiplicity' [14] originated from the study of *P*660*s* at MDJ, the same station as we use here, with seismograms selected to be from Tonga earthquakes only. For all these seismograms, *P*660*s* conversion points fall into our Sector II. In agreement with the earlier study, we observe that *P*660*s* arrivals in this sector are followed by two or three coherent arrivals of smaller amplitude, clearly visible on both the individual traces and stacks. In contrast to that study, however, we compare the location of the *P*660*s* conversion points with the inferred location of the subducting slab at the *660* and observe that the two do not coincide. We also use a broader range of azimuths and show that the arrivals of the *P*660*s* waves that do convert within the cold slab (Sector IV) are not followed by coherent peaks similar to those in Sector II, as would be expected if the peaks were the signal

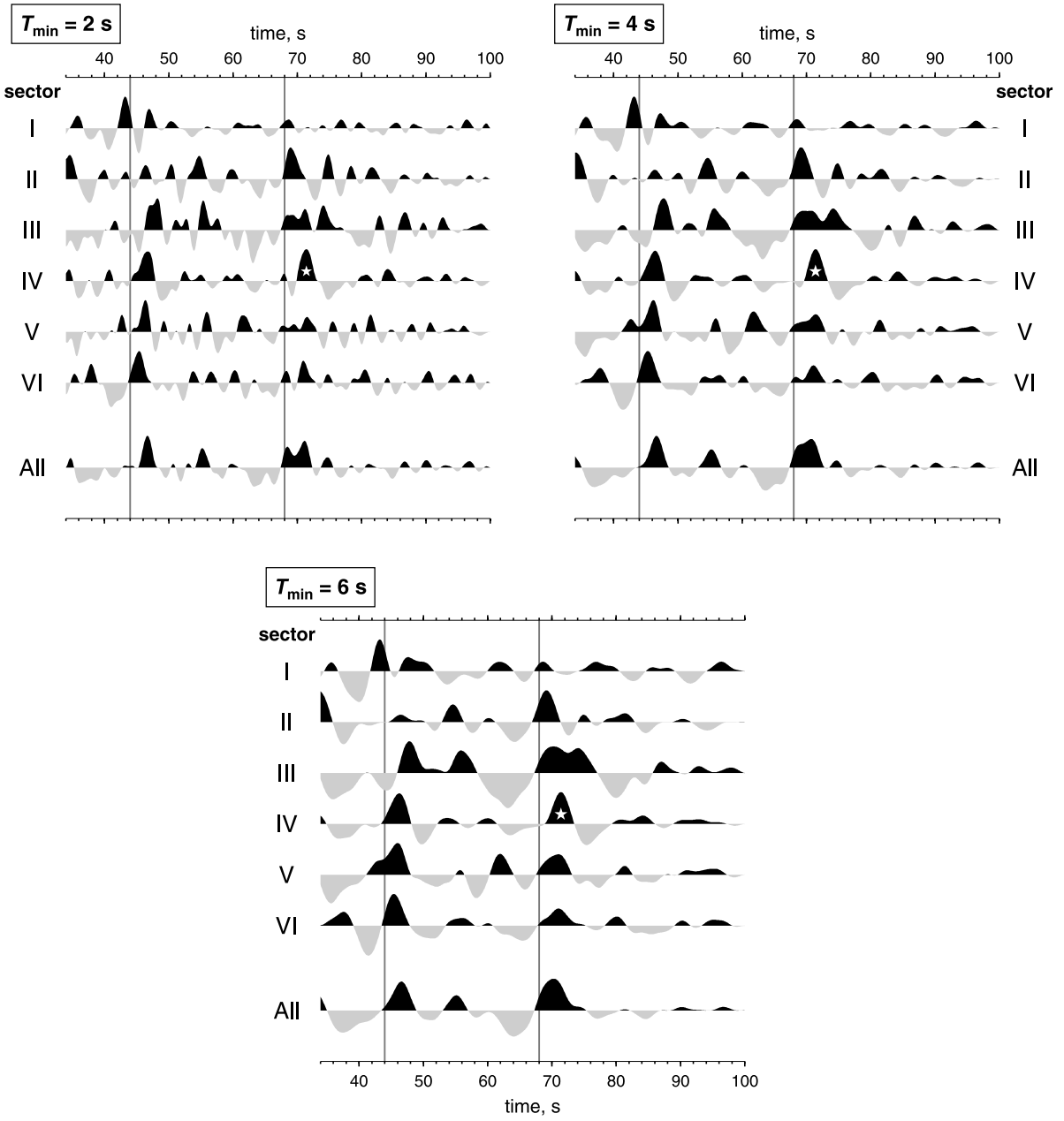

Fig. 7. The stacks of the traces in the six sectors defined in Figs. 4 and 5 (I–VI) and of all 134 traces (All). The stacked traces in the three frames are low-pass filtered at T_{min} of 2, 4, and 6 s. The stack value at each point is a sum of individual-trace values divided by the number of traces in the group. Global-average arrival times of *P*410*s* and *P*660*s* are marked with lines at 44 and 68 s. Star denotes the arrival of the *P*660*s* wave converted within the coldest part of the slab (Sector IV).

from additional discontinuities. Because the hypothetical discontinuities associated with the $gt \rightarrow il \rightarrow pv$ transformations are thought to exist at relatively low temperatures, they can be expected to be as prominent in the (coldest) Sector IV as in Sector II. The absence of any signal from them in Sector IV suggests that the multiple arrivals in Sector II are likely to be due either to a particular pattern of multipathing in this narrow range of azimuths, or to conversions from small-scale heterogeneity in the uppermost lower mantle in this particular location (possibly, the high-velocity features seen in Fig. 3 to the east of the slab, or the yet unexplained low-velocity feature immediately below the slab).

Although the accuracy of the *P*660*s* arrival-time measurements at MDJ is uncertain (because of the effect of the small-scale *660* topography on the waveforms), the general pattern of arrivals in different sectors is consistent with our estimate of the slab's location and with the thermal origin of the variations in the depth to the *660*. In particular, *P*660*s* from Sector IV (the coldest part of the slab) arrive more than 2 s later than those from Sector II (the warmer region outside or at the boundary of the slab), consistent with the expected deepening of the *660* at lower temperatures [22]. Perhaps the most surprising pattern in our data is the sharp contrast in the appearance of *P*660*s* waveforms in adjacent sectors (II and III; III and IV). Ray-theoretical conversion points within the sectors are only a few tens of kilometers away from the ones in the neighboring sectors. Fresnel zones of *P*660*s* are a few hundred kilometers wide (see [12] for a discussion on different estimates), and if they approximated the sensitivity volumes of the waves, then the waveforms corresponding to neighboring conversion points would be very similar. Clearly, this is not the case and there is no waveform similarity across sector boundaries (Figs. 4 and 5). Because of the presence of strong lateral heterogeneity, in particular small-scale topography on the *660* beneath MDJ, Fresnel zones do not describe the sensitivity of the waveforms to the Earth's structure. The *Pds* arrivals recorded at MDJ would make up a good dataset for future studies employing three-dimensional modeling of *Pds* propagation. Here, we use the ray-theoretical piercing points of *P*660*s* and *P*410*s* to approximately map the conversion locations and concentrate on our main argument: the *P*660*s* complexity results from lateral heterogeneity, in particular topography on the *660*, rather than from the presence of multiple discontinuities.

In agreement with our interpretation, extensive studies of the subduction-zone *660* with *S*660*P* waves (converted near the earthquake source) have also produced no evidence for multiple discontinuities near the *660*, showing, in contrast, that the discontinuity is sharp and simple [24].

Although the focus of this paper is on the *660*, we note that the appearance of the *P*410*s* phases also changes from sector to sector. In Sector II, there is no clear arrival, only a series of low-amplitude peaks near the expected *P*410*s* arrival time (Figs. 4 and 7). The subducting slab crosses the *410* more than 500 km east from MDJ, so if the waveform complexity is caused by variations in the depth to the *410*, these variations are not related to the probable uplift of the *410* within the slab. Alternatively, the signal can be explained by the distortion of the *P* wavefield below the *410*. If this is the case, then the origin of the multiple peaks in place of the *P*410*s* may be related to the origin of the multiple peaks following the *P*660*s* on the same traces. In Sectors II and III, we also observe coherent arrivals near 55 s, approximately where the signal from a (sharp) 520-km discontinuity would be. These arrivals, absent in Sector IV, could be conversions from a discontinuity at the top of the subducting slab. To arrive as early as 55 s, these conversions would have to occur east of the source–receiver great circle planes, where the slab is shallower (Fig. 5).

4. Conclusions

The *P*660*s* phases that convert from *P* to *s* at the *660* within the subducting NW-Pacific slab are remarkably clear and coherent, with no additional arrivals in the vicinity (Figs. 4 and 7). Conversions at the *660* near the boundaries of the slab produce distinctly more complex, multiple arrivals, with wave-propagation complexity (due to lo-

cal *660* topography) being the most plausible explanation. From within the coldest parts of the slab, we detect no signal that could be attributed to the hypothetical seismic discontinuities caused by the low-temperature $gt \rightarrow il \rightarrow pv$ phase transformations. These observations suggest that the phase transformations either do not occur in the mantle or are spread over tens of kilometers, without seismically visible sharp onsets. We also observe no clear short-period signal from the $gt \rightarrow pv$ transformation, consistent with its large effective width as estimated from mineral physics [7].

Acknowledgements

We thank Hrafnkell Kárason for computing the cross-sections through the tomographic model in Fig. 3, John Castle for a discussion on the near-source *S*660*P* conversions in subduction zones, and George Helffrich and an anonymous reviewer for comments and suggestions that helped us to improve the manuscript. Waveform data were provided by IRIS-DMC. Figures were prepared with GMT [28]. This work was supported by the David and Lucile Packard Foundation through a Fellowship awarded to R.D.v.d.H. ***[BW]***

References

[1] A.E. Ringwood, Phase transformations in the mantle, Earth Planet. Sci. Lett. 5 (1969) 401–412.
[2] E. Ito, E. Takahashi, Postspinel transformations in the system Mg_2SiO_4-Fe_2SiO_4 and some geophysical implications, J. Geophys. Res. 94 (1989) 10637–10646.
[3] J.E. Vidale, H.M. Benz, Upper-mantle seismic discontinuities and the thermal structure of subduction zones, Nature 356 (1992) 678–683.
[4] M.P. Flanagan, P.M. Shearer, Global mapping of topography on transition zone velocity discontinuities by stacking SS precursors, J. Geophys. Res. 103 (1998) 2673–2692.
[5] S. Lebedev, S. Chevrot, R.D. van der Hilst, Seismic evidence for olivine phase changes at the 410- and 660-kilometer discontinuities, Science 296 (2002) 1300–1302.
[6] D.J. Weidner, Y. Wang, Phase transformations: implications for mantle structure, in: S. Karato, A.M. Forte, R.C. Liebermann, G. Masters, L. Stixrude (Eds.), Earth's Deep Interior: Mineral Physics and Tomography From the Atomic to the Global Scale, AGU, Geophys. Monogr. 117 (2000) 215–235.
[7] L. Stixrude, Structure and sharpness of phase transitions and mantle discontinuities, J. Geophys. Res. 102 (1997) 14835–14852.
[8] P. Vacher, A. Mocquet, C. Sotin, Computation of seismic profiles from mineral physics: the importance of the non-olivine components for explaining the 660 km depth discontinuity, Phys. Earth Planet. Int. 106 (1998) 275–298.
[9] L.P. Vinnik, Detection of waves converted from P to SV in the mantle, Phys. Earth Planet. Int. 15 (1977) 39–45.
[10] H. Paulssen, Evidence for a sharp 670-km discontinuity as inferred from *P*-to-*S* converted waves, J. Geophys. Res. 93 (1988) 10489–10500.
[11] K. Stammler, R. Kind, N. Petersen, G. Kosarev, L. Vinnik, Q. Liu, The upper mantle discontinuities: correlated or anticorrelated?, Geophys. Res. Lett. 19 (1992) 1563–1566.
[12] S. Chevrot, L. Vinnik, J.-P. Montagner, Global scale analysis of the mantle *Pds* phases, J. Geophys. Res. 104 (1999) 20203–20219.
[13] S. Van der Lee, H. Paulssen, G. Nolet, Variability of *P*660*s* phases as a consequence of topography of the 660-km discontinuity, Phys. Earth Planet. Int. 86 (1994) 147–164.
[14] F.L. Niu, H. Kawakatsu, Complex structure of mantle discontinuities at the tip of the subducting slab beneath Northeast China – A preliminary investigation of broadband receiver functions, J. Phys. Earth 44 (1996) 701–711.
[15] N.A. Simmons, H. Gurrola, Multiple seismic discontinuities near the base of the transition zone in the Earth's mantle, Nature 405 (2000) 559–562.
[16] J. Castillo, A. Mocquet, G. Saracco, Wavelet transform: a tool for the interpretation of upper mantle converted phases at high frequency, Geophys. Res. Lett. 28 (2001) 4327–4330.
[17] R.D. Van der Hilst, E.R. Engdahl, W. Spakman, G. Nolet, Tomographic imaging of subducted lithosphere below northwest Pacific island arcs, Nature 353 (1991) 37–43.
[18] R. Van der Voo, W. Spakman, H. Bijwaard, Mesozoic subducted slabs under Siberia, Nature 397 (1999) 246–249.
[19] H. Kárason, R.D. van der Hilst, Constraints on Mantle Convection from seismic tomography, in: M.A. Richards, R.G. Gordon, R.D. van der Hilst (Eds.), The History and Dynamics of Global Plate Motions, AGU, Geophys. Monogr. 121 (2000) 277–288.
[20] Ó. Gudmundsson, M. Sambridge, A regionalized upper mantle (RUM) seismic model, J. Geophys. Res. 103 (1998) 7121–7136.
[21] M.M. Deal, G. Nolet, Slab temperature and thickness from seismic tomography 2. Izu-Bonin, Japan, and Kuril subduction zones, J. Geophys. Res. 104 (1999) 28803–28812.
[22] C.R. Bina, G.R. Helffrich, Phase transition Clapeyron slopes and transition zone seismic discontinuity topography, J. Geophys. Res. 99 (1994) 15853–15860.

[23] J.D. Collier, G.R. Helffrich, B.J. Wood, Seismic discontinuities and subduction zones, Phys. Earth Planet. Int. 127 (2001) 35–49.
[24] J.C. Castle, K.C. Creager, Local sharpness and shear wave speed jump across the 660-km discontinuity, J. Geophys. Res. 105 (2000) 6191–6200.
[25] E.R. Engdahl, R.D. van der Hilst, R. Buland, Global teleseismic earthquake relocation with improved travel times and procedures for depth determination, Bull. Seismol. Soc. Am. 88 (1998) 722–743.
[26] B.L.N. Kennett, E.R. Engdahl, R. Buland, Constraints on seismic velocities in the Earth from traveltimes, Geophys. J. Int. 122 (1995) 108–124.
[27] B.L.N. Kennett, E.R. Engdahl, Travel times for global earthquake location and phase identification, Geophys. J. Int. 105 (1991) 429–465.
[28] P. Wessel, W.H.F. Smith, New version of the Generic Mapping Tools released, EOS Trans. AGU 76 (1995) 329.